Journal of Applied Electrochemistry **34**: 963–969, 2004.
© 2004 *Kluwer Academic Publishers. Printed in the Netherlands.*

Reduction characteristics of iodate ion on copper: Application to copper chemical mechanical polishing

M. ANIK
Metallurgy Institute, Osmangazi University, 26480 Eskisehir, Turkey (e-mail: manik@ogu.edu.tr)

Received 18 August 2003; accepted in revised form 26 May 2004

Key words: CMP, copper, diffusion, iodate, kinetics

Abstract

Potentiodynamic and potentiostatic polarization, and the rotating disk electrode technique were used to study the reduction characteristics of iodate (IO_3^-) ion on copper (Cu). Depending on the relative concentrations of IO_3^- and H^+ two pH regimes were observed. The cathodic current in the first regime ($pH > 3$) was controlled by H^+ diffusion from the solution to the metal surface. In the second regime ($pH < 3$ and up to 10^{-2} M IO_3^- concentration) the cathodic current was found to be under mixed control, involving reaction control via the electrochemical reduction of IO_3^- and transport control via the diffusion of I_2 (aq). It was concluded that IO_3^- was an effective oxidant for Cu chemical mechanical polishing (CMP) with strongly acidic ($pH < 3$) slurries but it was not convenient reagent as an oxidant for Cu CMP with weakly acidic ($pH > 3$) slurries.

List of symbols

- n total number of electrons (mol^{-1})
- F Faraday constant (96 480 C mol^{-1})
- m reaction order for the reactant
- k apparent rate constant ($cm^{3m-2}\,s^{-1}\,mol^{1-m}$)
- C_b bulk concentration of the reactant (mol cm^{-3})
- α apparent charge transfer coefficient
- z number of electrons in the rate determining step
- R universal gas constant (8.314 J $mol^{-1}\,K^{-1}$)
- T absolute temperature (K)
- η overpotential (V)
- D diffusion coefficient of the reactant ($cm^2\,s^{-1}$)
- v kinematic viscosity (0.01 $cm^2\,s^{-1}$ for water)
- ω angular velocity (s^{-1}).

1. Introduction

Copper (Cu) is considered as the most promising interconnecting material in integrated circuits due to its low resistivity and high electromigration performance [1]. The integration of Cu technology into the device manufacturing process is possible by using the dual damascene technique [1] in which chemical–mechanical polishing (CMP) is employed to remove excess Cu from the field areas and planarize the surface for further processing [1].

Copper CMP slurries generally contain an oxidant, an etchant, and abrasive particles to obtain a polishing mechanism in which an oxide layer forms on the metal surface under the chemical action of the oxidant, and this oxide layer is then removed mechanically by the abrasive particles [2]. According to this mechanism, the effectiveness of a CMP process depends on the formation kinetics of an oxide layer and thus reduction kinetics of an oxidant on the metal surface. Therefore, the selection of an oxidant is an important issue in the design of a CMP process.

The iodate (IO_3^-) ion is an important oxidant in CMP [3–12]. The effectiveness of this reagent as an oxidant was explored via *in situ* electrochemical experiments at around pH 4 (typical IO_3^- concentration range is 10^{-2}–10^{-1} M) [3, 5, 10–12]; however, detailed investigation of the reduction behavior of IO_3^- was not conducted. A fundamental understanding of iodate-based Cu CMP can only be attained by highlighting how the reduction characteristics of IO_3^- on Cu depend on pH, IO_3^- concentration and rotation rate.

The electrochemical literature does not appear to contain any systematic studies on IO_3^- reduction on Cu. The reduction behavior of IO_3^- on platinum (Pt), however, has been characterized by many workers [13–21]. In this study, IO_3^- reduction on Cu is investigated by potentiodynamic and potentiostatic polarization, and the rotating disc electrode (RDE) technique. The accumulated insights on IO_3^- reduction on Pt are utilized in the interpretation of the results.

2. Background

The direct reduction of IO_3^- on Pt in acidic solutions is a slow process [14–16]:

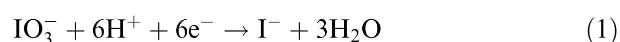

$$IO_3^- + 6H^+ + 6e^- \rightarrow I^- + 3H_2O \qquad (1)$$

However, I^- produced in this slow reaction (Equation 1) diffuses from the Pt surface and reacts rapidly with IO_3^- in the solution to form $I_2(aq)$:

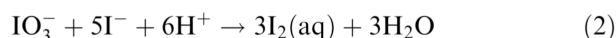

$$IO_3^- + 5I^- + 6H^+ \rightarrow 3I_2(aq) + 3H_2O \quad (2)$$

The $I_2(aq)$ formed in Equation 2 is transported to the electrode surface and reduces to I^-, setting up a catalytic loop:

$$I_2(aq) + 2e^- = 2I^- \quad (3)$$

The occurrence of the chemical reaction between IO_3^- and I^- (Equation 2) was confirmed by Desideri [14], who observed that the addition of complexing agents for I^- (like mercuric ion) shifted the IO_3^- wave towards more negative potentials. Another observation made by Desideri [14–16] was that IO_3^- reduction on pre-reduced Pt takes place in the potential range where I_2 reduction occurs and addition of I_2 promotes the reduction of IO_3^-.

Beran and Bruckenstein [17, 18] also studied the effect of I_2 on the catalytic reduction of IO_3^-. They concluded that addition of I_2 increases the rate of surface coverage of I_{ads} on the metal surface and thus generation of I^- (Equation 1) in the diffusion layer to promote Reaction 2 becomes faster.

In addition to Reactions 1–3, the following reactions also take place in solutions with high I^- concentration [22]:

$$I_2 + I^- = I_3^- \quad (4)$$

$$I_3^- + 2e^- = 3I^- \quad (5)$$

3. Materials and methods

3.1. *Materials*

A copper (Cu) rod 0.635 cm in diameter (99.998% purity) was obtained from Aldrich. Reagent grade KIO_3, K_2SO_4 and H_2SO_4 were purchased from Aldrich. All the aqueous solutions were prepared from doubly distilled water. The water was deoxygenated by bubbling argon before experiments and purging was continued throughout the experiments. All test solutions contained 0.1 M K_2SO_4 as a supporting electrolyte. The pH of the test solutions was adjusted with H_2SO_4.

3.2. *Methods*

The Cu electrode used in the electrochemical experiments was embedded in a cylindrical piece of Teflon. To block the crevice between the Teflon holder and the electrode (microstop lacquer was not effective in sealing the crevice and acetone was observed to dissolve the lacquer during cleaning of the specimen), epoxy was applied and subsequently allowed to harden in vacuum. The exposed electrode surface (0.317 cm^2) was ground with 1200 grit grinding paper and polished with 1 μm diamond paste just prior to each experiment. The polished electrode was rinsed with acetone and double distilled water to eliminate traces of diamond paste from the surface.

A standard three-electrode system consisting of a working electrode (copper), a counter electrode (platinum wire mesh), and a reference electrode (saturated calomel electrode) was used. The counter electrode was separated from the main compartment by enclosing it in a fritted glass tube. A Gamry model PC4/300 mA potentiostat/galvanostat controlled by a computer with a model DC105 DC Corrosion Analysis software was used in the electrochemical measurements. Rotating disc electrode (RDE) experiments were carried out using an EG&G model 616 rotating assembly. The electrical connection was provided from the back of the electrode by attaching it to the RDE assembly. All experiments were performed in a 200 ml glass cell.

Potentiodynamic polarization curves were generated by sweeping the potential from open circuit potential (the electrode was held for 1 h at the open circuit potential to allow steady-state to be achieved) to -1.4 V at a scan rate of 1 mV s^{-1} at rotation speeds of 0 and 1000 rpm. Potentiostatic polarization was carried out at -800 mV at 1000 rpm; the current initially showed a short transient behavior upon applying a potential step, followed by a steady-state current. In the RDE experiments the rotation rate was varied between 300 and 3000 rpm, with increments of 200 or 500 rpm. Unless indicated otherwise, all potentials are referred to the saturated calomel reference electrode, SCE (SCE, $+0.241$ V vs SHE). All experiments were conducted at laboratory temperature (25 ± 0.5 C).

4. Results and discussion

4.1. *Electrochemical equilibria in the I–H_2O and Cu–H_2O systems*

The relative stability regions of the aqueous substances in the I–H_2O system are shown in the potential (Eh)–pH diagrams (first provided by Pourbaix [23]), presented in Figure 1a and b for $[I] = 10^{-3}$ and 10^{-1} M, respectively (where [I] represents the concentration of total dissolved iodide). The data used to prepare these diagrams are tabulated in Table 1 [23, 24]. As shown in the diagrams, at very high potentials protonated and deprotonated forms of IO_4^- and IO_5^{3-} are the main I (VII) species in the acidic and basic regimes, respectively. A relatively small $HIO_4(aq)$ region appears below pH 1.6. At lower potentials, I (V) exists as HIO_3 below pH 1 and as IO_3^- above this pH. The reduction products of IO_3^-, i.e., I_2 and I^-, appear (just below the upper water stability line) in Figure 1a. In Figure 1b, which is based on a higher iodide concentration, a narrow region of I_3^- sandwiched

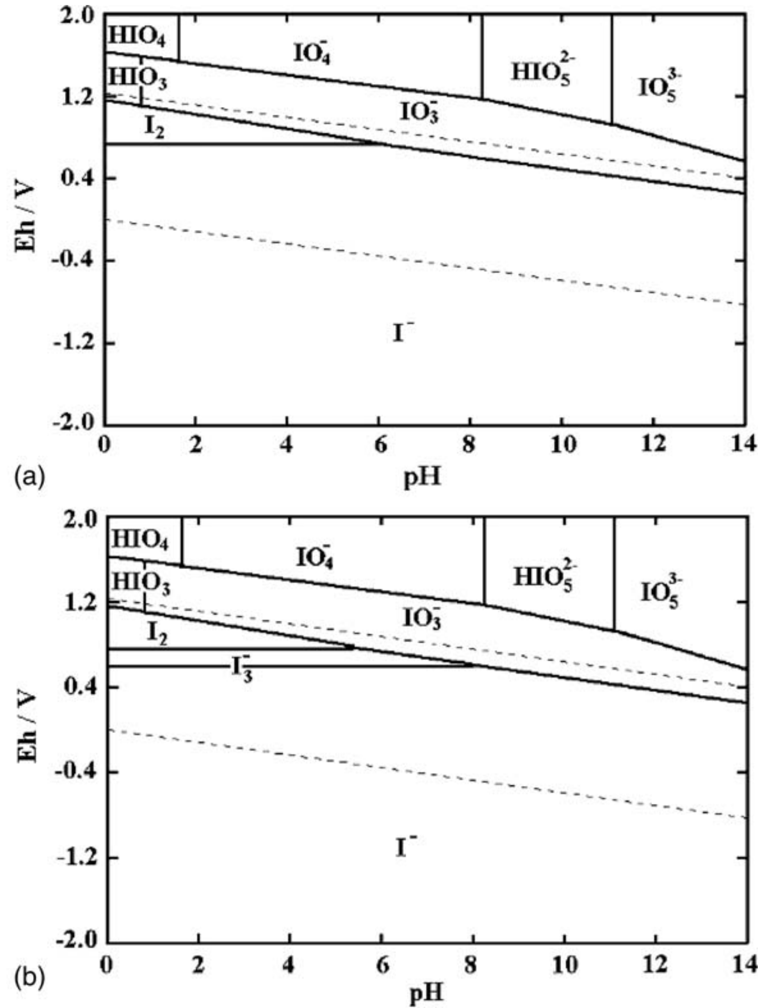

Fig. 1. Eh–pH diagrams for the I–H_2O system: (a) 10^{-3} M I and (b) 10^{-1} M I.

Table 1. Thermodynamic data for the I–H_2O and Cu–H_2O systems [23–25]

Reactions	E°/V	Log K
$HIO_4(aq) + 7H^+ + 8e^-$ $I^- + 4H_2O$	1.22	164
$IO_4^- + 8H^+ + 8e^-$ $I^- + 4H_2O$	1.23	166
$HIO_5^{2-} + 9H^+ + 8e^-$ $I^- + 5H_2O$	1.29	174
$IO_5^{3-} + 10H^+ + 8e^-$ $I^- + 5H_2O$	1.37	185
$HIO_3(aq) + 5H^+ + 6e^-$ $I^- + 3H_2O$	1.08	109
$IO_3^- + 6H^+ + 6e^-$ $I^- + 3H_2O$	1.09	110
$I_2(aq) + 2e^- = 2I^-$	0.62	21.0
$I_3^- + 2e^- = 3I^-$	0.54	18.1
$Cu^{2+} + 2e^- = Cu$	0.34	11.5
$2Cu^{2+} + H_2O + 2e^- = Cu_2O(s) + 2H^+$	0.203	7.0
$CuO(s) + 2H^+ = 2Cu^{2+} + H_2O$	–	7.3

between the I^- and I_2 domains is also observed. Comparison of Figure 1a and b reveals that the increase in the I concentration does not influence the positions of the equilibrium potentials considerably but it facilitates I_3^- formation in the I–H_2O system.

The potential–pH diagram for the Cu–H_2O system is depicted in Figure 2 (the dissolved metal concentration is fixed at 10^{-4} M). The related data are also provided in Table 1 [23, 25]. The cupric ion (Cu^{2+}) appears as a Cu dissolution product in the acidic regime. In neutral to basic solution, however, the formation of stable Cu_2O and CuO can be expected on the metal surface.

In the Cu–IO_3^- system, the porous CuI(s) formation is also evidenced by XPS characterization [10]. According to the electrochemical analysis, however, it is reported that the formation rate of CuI(s) is very slow and this rate can only be driven if the external I^- ion is added to the Cu–IO_3^- system [10].

Comparison of the equilibrium lines in Figures 1a, b and 2 (IO_3^-/I^-, I_2/I^-, I_3^-/I^-, Cu/Cu^{2+} and Cu/Cu_2O) shows that over very large IO_3^- concentration range (10^{-3}–10^{-1} M) and pH range (0–14) IO_3^- is a thermodynamically convenient oxidant for Cu.

4.2. *Potentiodynamic polarization experiments*

The cathodic polarization behavior of Cu with and without IO_3^- is shown in Figure 3a and b for pH 4 and 2, respectively, at 1000 rpm. The addition of IO_3^- in Figure 3a, does not change the corrosion current of Cu significantly. The cathodic current results from IO_3^- reduction and starts to increase at around −350 mV (after about 200 mV cathodic overpotential), reaching a

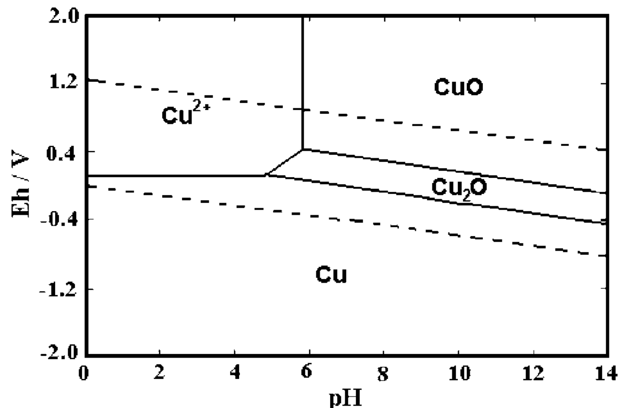

Fig. 2. Eh–pH diagram for Cu–H_2O system; [Cu] = 10^{-4} M.

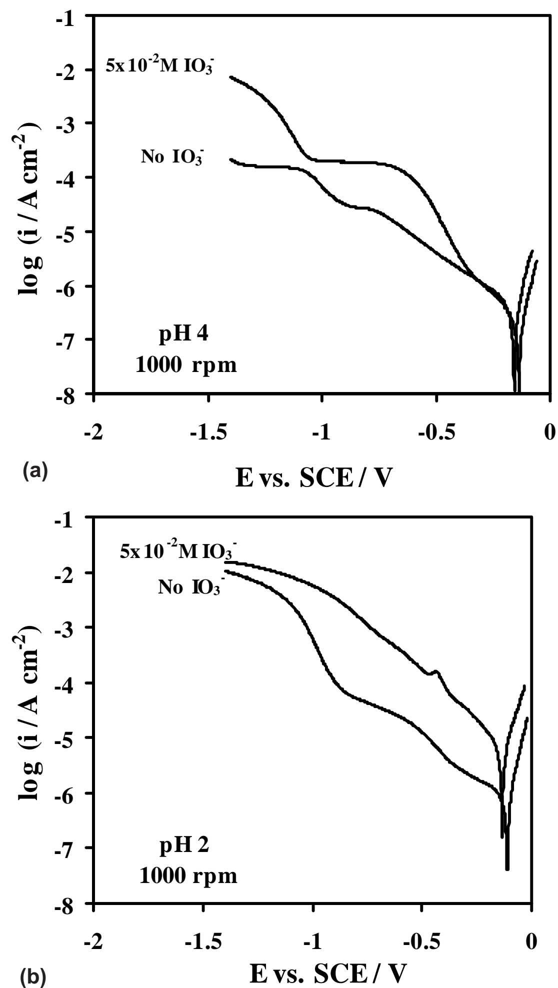

Fig. 3. Effect of IO_3^- on the cathodic polarization behavior of Cu at: (a) pH 4, and (b) pH 2, under 1000 rpm specimen rotation.

limiting value at around −700 mV. Below −1 V the increase in cathodic current re-commences due to the direct reduction of water on Cu since the local pH on the electrode surface increases at these high cathodic potentials.

The trends for pH 2, as illustrated in Figure 3b, are quite different from those in Figure 3a. The corrosion current of Cu increases with the addition of IO_3^- and the cathodic currents are higher in the presence of IO_3^- at all cathodic potentials. Also there is no limiting current for IO_3^- reduction.

The effect of the IO_3^- concentration on the corrosion potentials and corrosion currents in the pH range 2–4 is illustrated in Table 2. The change in both IO_3^- concentration and pH has no considerable influence on the corrosion potentials in this pH range. This result is not surprising since the Cu/Cu^{2+} equilibrium line in Figure 2 is pH independent and Cu dissolves in the active state in acidic solutions. The corrosion currents, however, increase as the IO_3^- concentration increases and the effect becomes more dramatic as the pH decreases.

4.3. *Potentiostatic polarization experiments*

The steady-state cathodic currents obtained at −800 mV at 1000 rpm specimen rotation for various pH and IO_3^- concentrations are shown as log *i* vs pH plots in Figure 4. In the generation of the plots in Figure 4, the background current (the cathodic current in the absence of IO_3^-) is subtracted from the cathodic current in the presence of IO_3^-. In other words, the cathodic currents in Figure 4 reflect solely the IO_3^- reduction current.

Two regimes may be recognized in Figure 4, depending on the relative concentrations of H^+ and IO_3^-. In the first regime (for all IO_3^- concentrations above pH 3 and for IO_3^- concentrations higher than 10^{-2} M below pH 3) cathodic currents are pH-dependent but do not vary with IO_3^- concentration. On the other hand, in the second regime (below pH 3 for IO_3^- concentrations less than 10^{-2} M) cathodic currents are sensitive to IO_3^- concentration, but the pH dependence is insignificant. The linear fit of cathodic current data for IO_3^- concentrations 2×10^{-2} and 5×10^{-2} M in Figure 4 shows that the reaction order for H^+ ion is 1 in the first regime.

Table 2. Effect IO_3^- concentration on the corrosion potential and corrosion current in the pH range 2–4

IO_3^- concentration	pH 2		pH 3		pH 4	
	E_{corr} vs. SHE (V)	i_{corr} (A cm^{-2})	E_{corr} vs. SHE (V)	i_{corr} (A cm^{-2})	E_{corr} vs. SHE (V)	i_{corr} (A cm^{-2})
10^{-2} M	0.107	3.0 10^{-6}	0.102	1.4 10^{-6}	0.095	8.0 10^{-7}
5 10^{-2} M	0.114	3.1 10^{-5}	0.103	1.3 10^{-5}	0.095	1.0 10^{-6}

Note that corrosion potentials are referred to standard hydrogen electrode (SHE)

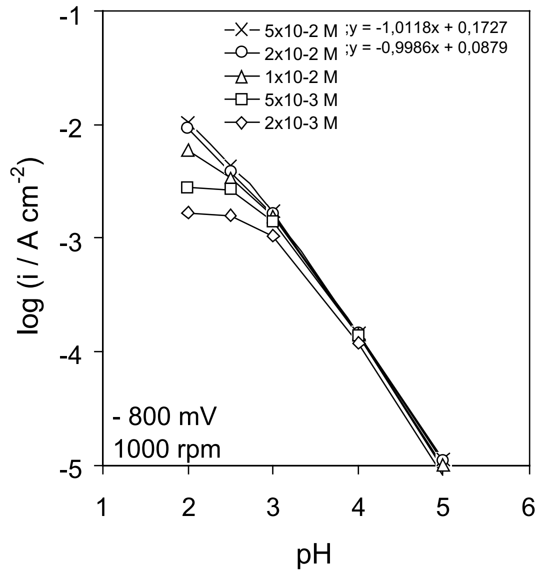

Fig. 4. Steady-state current vs pH.

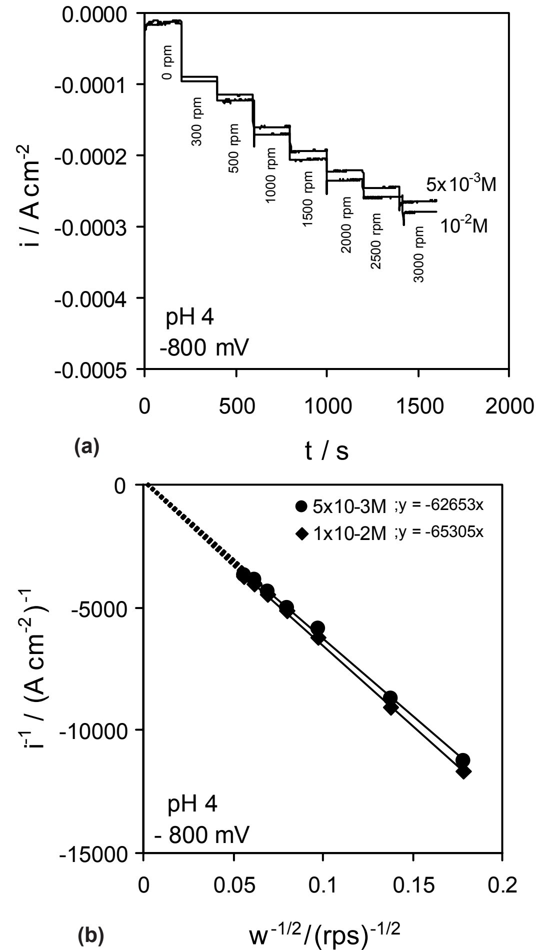

Fig. 5. (a) The effect of rotation on the steady-state cathodic currents at $-800\,\mathrm{mV}$ and pH 4 for various IO_3^- concentrations. (b) Corresponding i^{-1} vs $\omega^{-1/2}$ plots.

4.4. *Rotating disc electrode experiments*

The dependence of the steady-state cathodic current on the specimen rotation for $-800\,\mathrm{MV}$ and various IO_3^- concentrations at pH 4 (the first regime; Figure 4) is shown in Figure 5a. The corresponding Koutecky–Levich (i^{-1} vs $\omega^{-1/2}$) plots are given in Figure 5b. These plots are defined by Equation 6 for a first order reaction [26, 27]:

$$\frac{1}{i} = \frac{1}{i_K} + \frac{1}{i_D} \tag{6}$$

where i_K and i_D represent the kinetic- and diffusion-limited parts of the reduction current, respectively. Equations 7 and 8 provide expressions for i_K and i_D, respectively:

$$i_K = nFkC_b^m \exp\left(\frac{-z\alpha F\eta}{RT}\right) \tag{7}$$

$$i_D = 0.62nFD^{\frac{2}{3}}v^{\frac{-1}{6}}C_b\omega^{\frac{1}{2}} \tag{8}$$

Extrapolation of the currents to infinite rotation speed ($\omega \rightarrow \infty$; broken lines in Figure 5b) shows all the curves to intersect at the origin. This behavior suggests that the cathodic current in the first regime is totally diffusion controlled. Since the cathodic current is only sensitive to pH and the reaction order for H^+ is 1 (Figure 4) in the first regime, the diffusion control is associated with the slow diffusion of H^+ from the bulk of solution to the metal surface. This result is not surprising since Reactions 1 and 2 need high amount of H^+ to take place.

According to Equations 6 and 8, the slopes of the plots in Figure 5b provide the diffusion coefficient. If the activity coefficient of H^+ is assumed as 1, the diffusion coefficient of this ion is calculated as $4.5 \times 10^{-5}\,\mathrm{cm^2\,s^{-1}}$ from Figure 5b ($n = 1$ and $C_{bH+} = 10^{-7}\,\mathrm{mol\,cm^{-3}}$ at pH 4). This diffusion coefficient value is lower than the typical diffusion coefficient of H^+ ($9 \times 10^{-5}\,\mathrm{cm^2\,s^{-1}}$). If the slight influence of the IO_3^- concentration on the slopes of the plots in Figure 5b is considered, this calculated diffusion coefficient can be accepted as an effective diffusion coefficient of H^+ in the first regime.

The rotation dependence of the steady-state cathodic current in the second regime at $-800\,\mathrm{mV}$ and pH 2 for various IO_3^- concentrations is presented in Figure 6a. As the rotation rate increases, the cathodic current also increases. However, the increase in current with rotation in Figure 6a is not as significant as that in Figure 5a. Also when the IO_3^- concentration increases from 2×10^{-3} to $5 \times 10^{-3}\,\mathrm{M}$, the rate of increase in cathodic current with rotation decelerates. The corresponding Koutecky–Levich plots are given in Figure 6b. The plots show that the cathodic current in the second regime is under mixed control by kinetics and diffusion [26, 27].

The iodate concentration dependence of the cathodic currents in the second regime suggests that the kinetic control involved in the reduction must be associated with the direct reduction of IO_3^- as in Equation 1. In fact, the reduction of I_2 (Equation 3) is reversible and

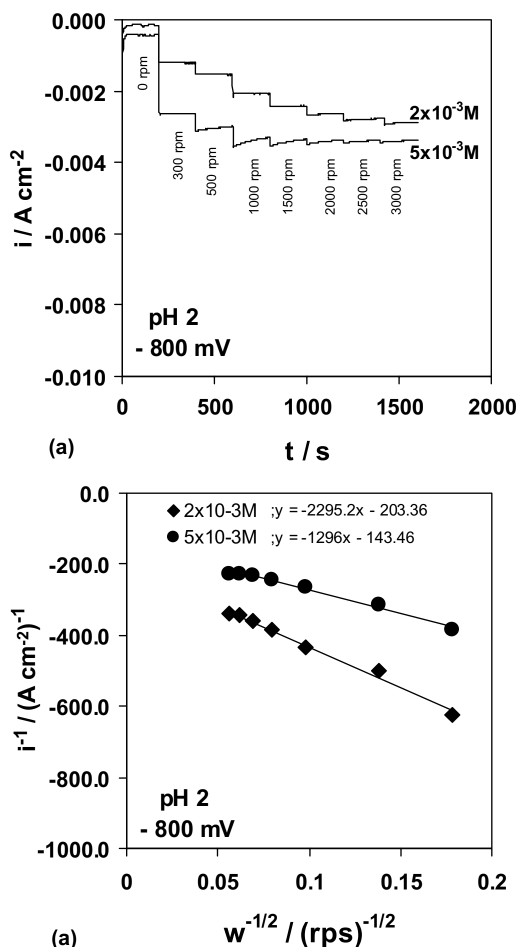

Fig. 6. (a) The effect of rotation on the steady-state cathodic currents at −800 mV and pH 2 for various IO_3^- concentrations. (b) Corresponding i^{-1} vs $\omega^{-1/2}$ plots.

purely diffusion controlled [22] so that it may be considered not to influence the kinetic steps in the reduction. The association of the kinetic steps with the direct reduction of IO_3^- in the catalytic loop (Equations 1–3) is also reported for IO_3^- reduction on Pt [21].

Extrapolation of the currents to infinite rotation speed ($\omega \rightarrow \infty$) in Figure 6b yields the kinetic currents (as printed on the figure) for both concentrations. These currents provide the values of m ($m = \partial \log i_K / \partial \log C_b$) and k in Equation 7 as approximately 0.4 and $10^{-6}\,cm^{-0.8}\,s^{-1}\,mol^{0.6}$, respectively. If z is assumed as 1, Equation 7 gives the value of α as 0.05 ($E_{eqm\ IO3-/I-} \cong$ 1.08–0.059 pH [24]). This value of α is not unusual for the IO_3^- reduction since the reduction mechanism of this ion involves the adsorption of iodine atoms at the electrode surface [24]. Therefore the reduction rate of IO_3^- strongly depends on the surface state of the electrode [21].

The diffusion control involved in the reduction in the second regime can be attributed to slow diffusion of I_2(aq) from the bulk solution to the metal surface to take part in Reaction 3 which couples to Reactions 1 and 2 to form a catalytic loop. The influence of diffusion control on the cathodic current decreases as the IO_3^- concentration increases as can be seen in Figure 6b (the slope of the plots decreases as the IO_3^- concentration increases [26, 27]). The increase in IO_3^- concentration increases the I_2(aq) formation at the metal–solution interface (through Reactions 1 and 2). In fact, in the second regime with the increase in IO_3^- concentration, it was observed in the present work that a solid I_2 (gray–black) layer formed on the surface of both the metal electrode and the Teflon holder (solubility limit of I_2 is 1.3×10^{-3} M [22]), supporting the catalytic loop expressed by Reactions 2 and 3. Therefore, increase in I_2(aq) concentration at the metal–surface interface may decrease the diffusion control of the cathodic current.

4.5. *Effectiveness of iodate as an oxidant for the Cu CMP*

The results obtained can be used in evaluation of the effectiveness of IO_3^- as an oxidant for the Cu CMP. Above pH 3 the presence of IO_3^- does not influence the corrosion current of Cu significantly and the reduction of IO_3^- on Cu commences only after a specific cathodic overpotential (Figure 3a). Also, increase in IO_3^- concentration does not affect the cathodic process (Figure 4; the first regime). Obviously IO_3^- does not appear to be a suitable oxidant for the Cu CMP in the weakly acidic slurries. This observation is very important since if the pH for the commercial IO_3^- based CMP slurry, which contain as high as 10^{-1} M IO_3^-, is selected as 4 [3, 5, 10–12], IO_3^- in this slurry does not act as an effective oxidant for Cu.

Below pH 3, however, IO_3^- reduction on Cu takes place at a significant rate and the Cu corrosion rate increases with addition of IO_3^- (Figure 3b). Increase in IO_3^- concentration up to 2×10^{-2} M, increases the cathodic current (Figure 4; the second regime). Therefore in this pH regime IO_3^- acts as an effective CMP oxidant and the increase in the IO_3^- concentration (up to 2×10^{-2} M) of the slurry increases the chemical contribution to the Cu CMP.

The typical linear velocity range of the polishing pad is 20–100 cm s^{-1} for the CMP process [1]. The increase in the linear velocity of the polishing pad can also be expected to improve the chemical contribution to the Cu CMP in the IO_3^- based slurries since the rate of the IO_3^- reduction on Cu is partly controlled by diffusion. These predictions, of course, should be checked by polishing experiments.

5. Summary and conclusions

The reported data on the reduction behavior of IO_3^- on Cu are very limited in the literature. Therefore, it is believed that the present work has provided the first systematic analysis of the IO_3^- reduction characteristics on Cu. In addition, the data generated will be helpful in advancing fundamental understanding of iodate-based Cu CMP. The results obtained are summarized below:

- The dependence of the steady-state cathodic currents on pH at various IO_3^- concentrations showed that

there are two regimes. In the first regime (pH > 3) the cathodic currents were pH-dependent but did not vary with IO_3^- concentration, and in the second regime (pH < 3 and up to 10^{-2} M IO_3^- concentration) the cathodic currents were sensitive to IO_3^- concentration but pH dependence was insignificant.

- The cathodic current in the first regime was controlled by H^+ diffusion from the solution to the metal surface.
- In the second regime the cathodic current was found to be under mixed control, involving reaction control via the electrochemical reduction of IO_3^- and transport control via the diffusion of I_2.
- IO_3^- was estimated as an effective oxidant for Cu chemical mechanical polishing (CMP) with strongly acidic (pH < 3) slurries but it was not convenient as an oxidant for Cu CMP with weakly acidic (pH > 3) slurries.

Acknowledgement

This work was supported by the Turkish State Planning Organization (Project Number: 2002K120550).

References

1. J.M. Steigerwald, S.P. Murarka and R.J. Gutmann, 'Chemical Mechanical Planarization of Microelectronic Materials' (Wiley, New York, 1997), p. 209.
2. F.B. Kaufman, D.B. Thompson, R.E. Broadie, M.A. Jaso, W.L. Guthrie, D.J. Pearson and M.B. Small, *J. Electrochem. Soc.* **138** (1991) 3460.
3. E.A. Kneer, C. Raghunath, V. Mathew, S. Raghavan and J.S. Jeon, *J. Electrochem. Soc.* **144** (1997) 3041.
4. H. van Kranenburg and P.H. Woerlee, *J. Electrochem. Soc.* **145** (1998) 1285.
5. D.J. Stein, D. Hetherington, T. Guilinger and J.L. Cecchi, *J. Electrochem. Soc.* **145** (1998) 3190.
6. Y.L. Wang, C. Liu, C. Liu, M.S. Feng and W.T. Tseng, *Mat. Chem. Phys.* **52** (1998) 17.
7. D.J. Stein, D.L. Hetherington and J.L. Cecchi, *J. Electrochem. Soc.* **146** (1999) 376.
8. D. Tamboli, S. Seal, V. Desai and A. Maury, *J. Vac. Sci. Technol. A* **17** (1999) 1168.
9. K. Osseo-Asare, M. Anik and J. DeSimone, *Electrochem. Solid-State Lett.* **2** (1999) 143.
10. S.M. Lee, U. Mahajan, Z. Chen and R.K. Singh, in Y.A. Arimoto, R.L. Opila, C.R. Simpson, K.B. Sundaram, I. Ali and Y. Homma (eds.), 'Chemical Mechanical Polishing in IC Device Manufacturing III', PV 1999-37 (Electrochem. Soc. Proc. Pennington, NJ, 2000), p. 187.
11. M. Anik and K. Osseo-Asare, in Y.A. Arimoto, R.L. Opila, C.R. Simpson, K.B. Sundaram, I. Ali and Y. Homma (eds.), 'Chemical Mechanical Polishing in IC Device Manufacturing III', PV 1999-37 (Electrochem. Soc. Proc. Pennington, NJ, 2000), p. 354.
12. M. Anik and K. Osseo-Asare, in P.C. Andricacos, J.L. Stickney, P.C. Searson, C. Reidsema-Simpson and G.M. Oleszek (eds.), 'Electrochemical Processing in ULSI Fabrication III', PV 2000-8 (Electrochem. Soc. Proc. Pennington, NJ, 2002), p. 234.
13. F.C. Anson, *J. Am. Chem. Soc.* **81** (1959) 1554.
14. P.G. Desideri, *J. Electroanal. Chem.* **9** (1965) 218.
15. P.G. Desideri, *J. Electroanal. Chem.* **9** (1965) 229.
16. P.G. Desideri, *J. Electroanal. Chem.* **17** (1968) 129.
17. P. Beran and S. Bruckenstein, *J. Phys. Chem.* **72** (1968) 3630.
18. P. Beran and S. Bruckenstein, *Anal. Chem.* **40** (1968) 1044.
19. L. Muller, *J. Electroanal. Chem.* **16** (1968) 67.
20. L. Muller, *J. Electroanal. Chem.* **16** (1968) 531.
21. B.R. Wels, D.S. Austin-Harrison and D.C. Johnson, *Langmuir* **7** (1991) 559.
22. K.J. Vetter, 'Electrochemical Kinetics' (Academic Press, New York, 1967), p. 399.
23. M. Pourbaix, 'Atlas of Electrochemical Equilibria in Aqueous Solutions' (Pergamon, London, 1966), p. 384, 614.
24. P.G. Desideri, L. Lepri and D. Heimler, in A.J. Bard (ed.), 'Encyclopedia of Electrochemistry of the Elements, Vol. 1 (Marcel Dekker, New York, 1973), p. 91.
25. U. Bertocci and D.R. Turner, in A.J. Bard (ed.), 'Encyclopedia of Electrochemistry of the Elements', Vol. 6 (Marcel Dekker, New York, 1977), p. 383.
26. A.J. Bard and L.R. Faulkner, 'Electrochemical Methods' (Wiley, New York, 1980), p. 280.
27. Yu. V. Pleskov and V. Yu. Filinovskii, 'The Rotating Disc Electrode' (Plenum, New York, 1976), p. 84.